Orissa Journal of Physics
ISSN 0974-8202

Vol. 33, No.1
February 2026
pp. 56-67

Design and Numerical Simulation of Azetidinium-based Multi-Layer Perovskite Solar Cells Using SETFOS

PRANSU PRAGNYAN DASH [1], SUKANTA KUMAR TRIPATHY [1] and SUBRAT KUMAR SHADANGI [2†]

[1]*Centre of Excellence in Nano Science and Technology for Development of Sensors, P.G. Department of Physics, Berhampur University, Berhampur,760007, Odisha, India*
[2]*Department of Physics, Tara Tarini College, Purushottampur,761018, Odisha, India*

†Corresponding Author E-MAIL: shadangisubrat@gmail.com

Abstract: Solar photovoltaic technology continues to advance toward higher efficiency and lower-cost energy solutions, with metal–halide perovskites emerging as leading candidates for next-generation solar cells. While conventional perovskite absorbers offer excellent optoelectronic properties and have rapidly achieved efficiencies above 26%, their long-term instability remains a major barrier to commercialisation. Multi-absorber and tandem perovskite architectures present an effective strategy to enhance spectral utilisation and device durability beyond the single-junction limit. In this study, we explore Azetidinium (AZ^+) as a novel A-site cation for stabilising multi-absorber perovskite structures. The unique four-membered cyclic geometry of AZ^+ improves lattice rigidity, enhances moisture and thermal resistance, suppresses ion migration, and promotes uniform crystallisation. These characteristics yield reduced defect density and improved carrier transport, making AZ-based perovskites highly suitable for high-efficiency, stable tandem configurations. Our findings highlight Azetidinium as a promising pathway toward robust, commercially viable next-generation perovskite photovoltaics. The proposed configuration of the PSC consists of $FTO/SnS_2/AZSnBr_3/AZSnI_3/Cu_2O/Au$. Where Azetidinium Tin Bromide ($AZSnBr_3$) and Azetidinium Tin Iodide ($AZSnI_3$) are the absorber layers. Tin Disulfide (SnS_2) and Cuprous Oxide (Cu_2O) are the electron transport layer (ETL) and hole transport layer (HTL), respectively. Fluorine-doped Tin Oxide (FTO) and Gold (Au) are typically utilised as top and bottom electrodes, respectively. Using the Semiconducting Thin Film Optics Simulation (SETFOS) 5.3 software, the thicknesses of each layer were optimised to achieve a PCE of 23.91%, Fill Factor (FF) of 78.73%, Open Circuit Voltage (V_{OC}) of 0.74 V, Short Circuit Current Density (J_{SC}) of 40.99 mA/cm^2, and External Quantum Efficiency (EQE) of 93.68%.

Keywords: Perovskite, Multi-Absorber, Azetidinium, $AZSnBr_3$, $AZSnI_3$, Setfos.

INTRODUCTION

Solar photovoltaic (PV) technology has become one of the most transformative renewable energy solutions due to its ability to convert sunlight directly into electricity via the photovoltaic effect, offering a clean, abundant, and sustainable alternative to fossil fuels[1]. As energy demand continues to rise globally, solar cells have become indispensable in modern society, powering residential rooftop systems, remote sensors, agricultural irrigation setups, satellites, transportation systems, and large-scale solar farms[2]. Their silent operation, low maintenance, modularity, and suitability for remote regions make PV systems critical for both developed and developing countries[3]. The evolution of photovoltaic technology is typically divided into three generations. First-generation crystalline silicon (c-Si) cells dominate the global market due to their excellent durability and mature manufacturing processes, although they require energy-intensive fabrication[4]. Second-generation thin-film technologies, such as CdTe and CIGS, reduce material consumption and manufacturing costs, but their commercial expansion is limited by toxicity and elemental scarcity[5]. Third-generation solar cells—including dye-sensitised, organic, quantum-dot, and perovskite solar cells—aim to overcome the Shockley–Queisser limit using new materials with tunable band gaps and low-temperature fabrication[6]. While each generation offers unique benefits, no technology fully satisfies the combined requirements of high efficiency, low cost, scalability, environmental safety, and long-term stability.

Perovskite solar cells (PSCs) have emerged as the most promising third-generation PV technology due to their remarkable optoelectronic properties, including high absorption coefficients, long carrier diffusion lengths, sharp band edges, and defect tolerance[7]. Their power conversion efficiency has soared from 3.8% in 2009 to over 26% in recent certified devices[8-9]. Additionally, PSCs can be processed at low temperatures using scalable solution-based techniques, enabling the development of lightweight and flexible photovoltaic modules[10]. However, their commercial deployment is hindered by moisture and thermal instability, ion migration, structural softness, and environmental concerns surrounding the toxicity of lead[11]. Multi-absorber and tandem perovskite solar cells have emerged as a promising strategy to overcome efficiency and stability limitations. By stacking absorber layers with different band gaps, tandem architectures capture a wider portion of the solar spectrum, reduce thermalisation losses, and surpass single-junction efficiency limits[12]. Perovskite–silicon tandems have already exceeded 30% efficiency, and all-perovskite tandems are rapidly improving due to their bandgap tunability and compatibility with low-temperature processing[13]. The development of stable, selective absorber layers is central to achieving long-term operational stability and high efficiency in multi-absorber PSCs.

In this context, Azetidinium (AZ^+) has recently gained attention as a promising A-site cation for perovskite absorbers due to its unique molecular structure and stabilising effects. The four-membered ring of Azetidinium introduces stronger hydrogen bonding, improved lattice rigidity, and enhanced resistance to moisture and thermal degradation compared with methylammonium (MA^+), Formamidinium (FA^+), or Cesium (Cs^+)[14]. Azetidinium incorporation suppresses undesirable phase transitions, reduces ion migration, and promotes uniform crystallisation, resulting in perovskite films with lower defect density and improved carrier lifetimes. Furthermore, AZ-based perovskites exhibit tunable band gaps, making them ideal for high-performance multi-absorber and tandem architectures[15]. These unique advantages establish Azetidinium as a highly suitable absorber component for next-generation perovskite solar cells, addressing key challenges related to stability and performance.

SIMULATED DEVICE STRUCTURE

Using the AM 1.5G illumination spectrum, the optoelectronic performance of the proposed lead-free perovskite solar cell was numerically investigated employing SETFOS-5.3, a one-dimensional simulation tool widely used for thin-film photovoltaic devices. The simulated superstrate configuration consists of Glass/FTO/SnS_2/$AZSnBr_3$/$AZSnI_3$/Cu_2O/Au, where $AZSnBr_3$ acts as the primary absorber layer due to its suitable band gap and non-toxic nature, making it a promising alternative to conventional lead-based perovskites. SnS_2 and Cu_2O are selected as the electron transport layer (ETL) and hole transport layer (HTL), respectively, owing to their favourable band alignment, high carrier mobility, and compatibility with tin-based absorbers, while a thin $AZSnI_3$ interfacial layer is introduced to improve energy-level matching and reduce interfacial recombination losses. The simulation was conducted at 300 K over a wavelength range of 300–2500 nm, incorporating optical interference effects through the transfer-matrix method and solving the coupled Poisson and carrier continuity equations, which included Shockley–Read–Hall and radiative recombination mechanisms. FTO and Au were employed as the front and back electrodes, respectively. Proper conduction and valence band alignment across the ETL/absorber/HTL interfaces enables efficient charge separation, suppresses carrier recombination, and enhances charge extraction, consistent with previously reported SETFOS-based numerical studies on lead-free perovskite and Cu_2O heterojunction solar cells.

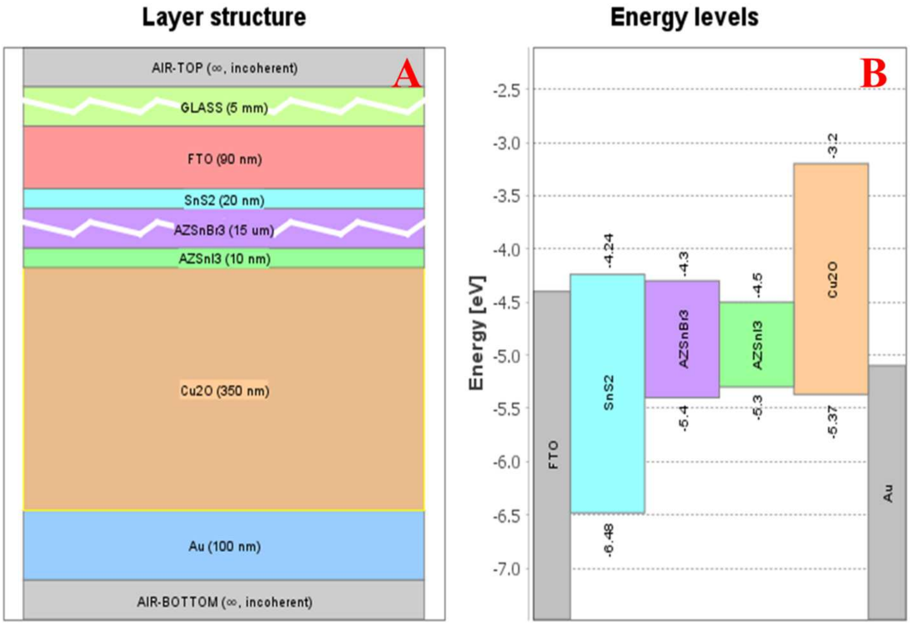

Figure 1. Represents the Simulated Device Structure with its respective Energy Levels.

Table 1. Represents the Input parameters used for PSC simulation.

	SnS_2	$AZSnBr_3$	$AZSnI_3$	Cu_2O
E_g (eV)	2.24	1.1	0.8	2.17
X (eV)	4.24	4.3	4.5	3.2
ε_r	10	16.3	16.3	7.5
N_L (cm^{-3})	2.2E18	1E19	1E19	2E18
N_H (cm^{-3})	1.8E19	1E19	1E19	1.1E19
N_A (cm^{-3})	0	5E16	5E16	2E19
N_D (cm^{-3})	1E18	5.21E9	5.21E9	0
μ_e(cm^2/Vs)	50	1.3	1.3	20
μ_p (cm^2/Vs)	50	1.3	1.3	80

RESULTS AND DISCUSSION

I. Effect of Absorber Layer on the Performance of the PSC:

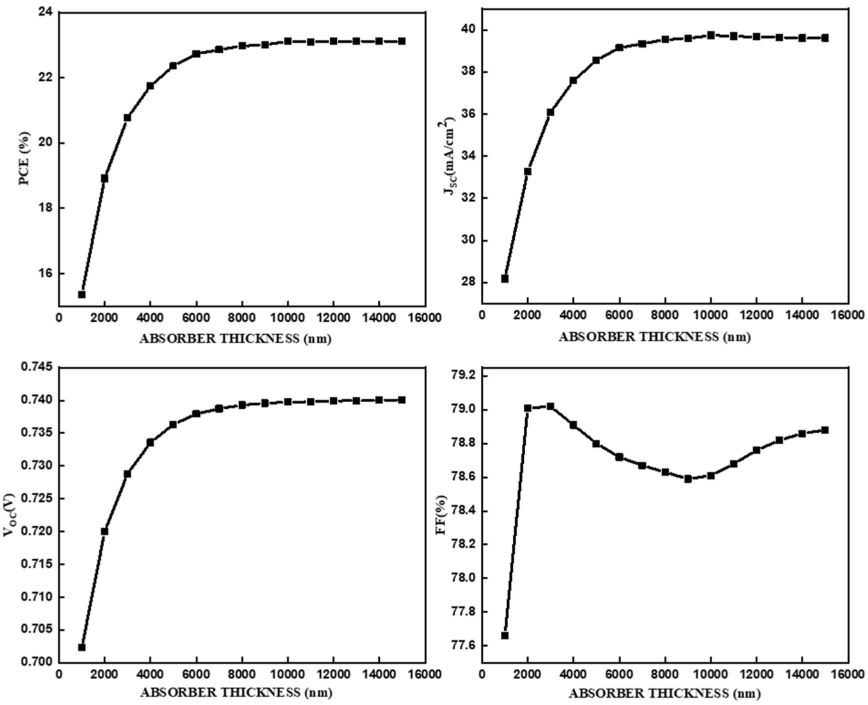

Figure 2. Represents the impact of the Absorber Layer thickness on the performance of the PSC.

To determine the optimal device structure, the absorber layer thickness was varied from 1 µm to 16 µm while keeping the transport layer parameters constant, as shown in Figure 2. The Short-Circuit Current Density (J_{SC}) and Power Conversion Efficiency (PCE) exhibit a rapid initial increase consistent with the Beer-Lambert law, eventually saturating at approximately 39.6 mA/cm^2 and 23.1%, respectively, for thicknesses exceeding 10 µm. This saturation indicates that the optical depth of the Sn-based absorber has been fully utilised to maximise photon harvesting. Although the Fill Factor (FF) peaks at ~ 3µm and experiences a minor decline due to increased series resistance in thicker films, the trade-off is negligible compared to the substantial gains in the current generation. Consequently, an absorber thickness of 15 µm was selected as the optimal value, ensuring complete optical absorption and maximising overall efficiency. It is essential to note that this optimal thickness assumes a material with high crystalline quality and low defect density, similar to single-crystal perovskites, where long carrier diffusion lengths enable efficient charge extraction even in thick films without significant recombination losses.

II. Effect of Passivation Layer on the Performance of the PSC:

Following the optimisation of the bulk absorber, the thickness of the $AZSnI_3$ passivation layer was varied from 10 nm to 100 nm to assess its impact on interface quality and charge extraction, as depicted in Figure 3. The Power Conversion Efficiency (PCE) and Short-Circuit Current Density (J_{SC}) exhibit a monotonic, albeit slight, decline as the layer thickness increases. Specifically, the PCE decreases from a maximum of 23.13% at 10 nm to 23.11% at 100 nm. This downward trend suggests that while a thin interfacial layer is beneficial for band alignment, increasing its thickness introduces parasitic absorption and additional series resistance, which hinders carrier collection. The Open-Circuit Voltage (V_{OC}) remains relatively stable, peaking subtly around 30 nm before degrading, further indicating that a thicker passivation layer may induce bulk recombination losses that outweigh the benefits of surface passivation. Consequently, a thickness of 10 nm was selected as the optimal value to maintain the highest efficiency while ensuring favourable energetic alignment at the back interface.

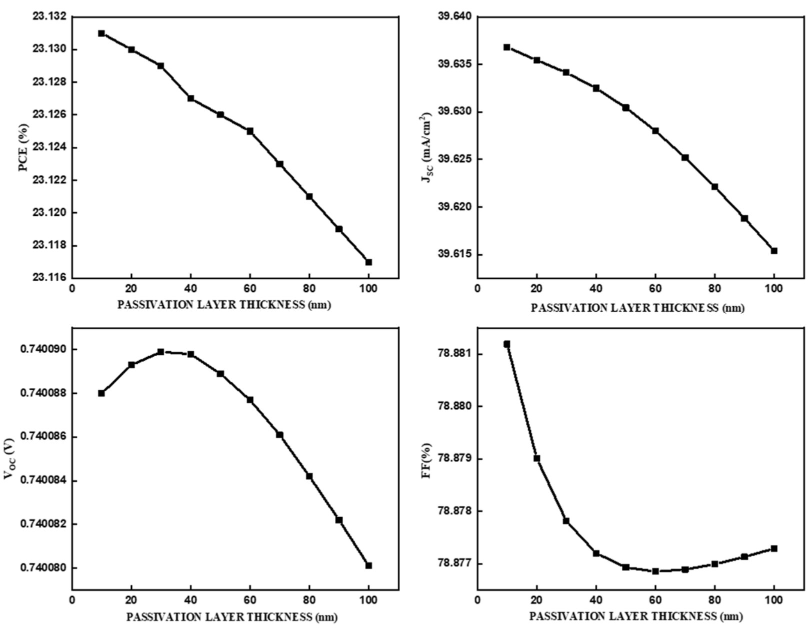

Figure 3. Represents the impact of the Passivation Layer thickness on the performance of the PSC.

III. Effect of Electron Transport Layer on the Performance of the PSC:

To further enhance device performance, the thickness of the SnS2 Electron Transport Layer (ETL) was optimised by varying it from 10 nm to 300 nm, as presented in Figure 4. Unlike the saturation behaviour observed in the absorber, the Short-Circuit Current Density (J_{SC}) and Power Conversion Efficiency (PCE) exhibit a distinct oscillatory pattern, characteristic of Fabry-Perot optical interference effects within the thin-film stack. The simulation reveals a primary efficiency maximum at a thickness of 20 nm, achieving a peak PCE of ~23.8% and JSC of 40.9 mA/cm2. This peak corresponds to a condition of constructive interference that maximises photon transmission into the absorber layer. A significant dip in performance is observed around 70 nm due to destructive interference, coupled with a localised peak in Fill Factor (FF). While the FF improves slightly in this region—likely due to reduced recombination current or improved shunting resistance—it is insufficient to compensate for the massive loss in photocurrent. Consequently, an ETL thickness of 20 nm was selected as the optimal value, ensuring minimal resistive losses while leveraging optical coupling to maximise current generation.

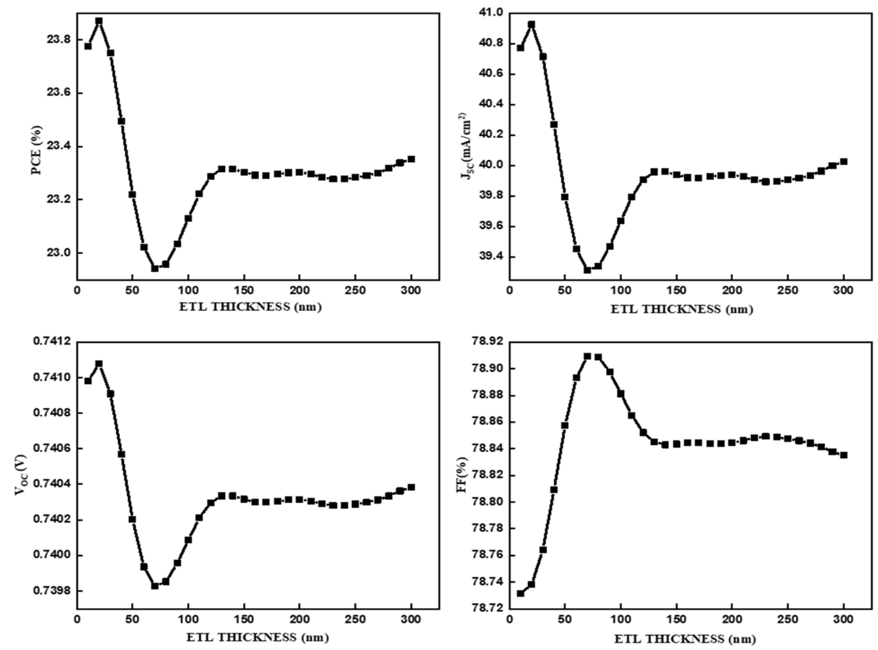

Figure 4. Represents the impact of the Electron Transport Layer thickness on the performance of the PSC

IV. Effect of Hole Transport Layer on the Performance of the PSC:

Finally, the thickness of the Cu_2O Hole Transport Layer (HTL) was optimised by varying it from 10 nm to 500 nm to determine the ideal balance between optical, electrical, and recombination losses, as shown in Figure 5. The Short-Circuit Current Density (J_{SC}) and Power Conversion Efficiency (PCE) display a smooth, quasi-sinusoidal variation, indicative of Fabry-Perot interference within the multilayer stack. A distinct performance maximum is observed at a thickness of 350 nm, where the PCE reaches 23.89% and J_{SC} peaks at 40.95 mA/cm^2. This peak corresponds to a condition of constructive interference, where the optical electric field is maximised within the absorber layer, enhancing photon harvesting. Conversely, the Fill Factor (FF) exhibits an inverse trend, reaching a local minimum at 350 nm. This reduction is attributed to the increased series resistance associated with the thicker oxide layer, which slightly impedes carrier extraction. However, the substantial gain in photocurrent at this optical resonance node outweighs the resistive losses in the fill factor. Consequently, a thickness of 350 nm was selected as the optimal value for the HTL.

V. Effect of Temperature on the Performance of the PSC:

To evaluate the thermal stability of the device under realistic operating conditions, the performance metrics were simulated as a function of temperature from 275 K to 350 K, as illustrated in Figure 6. The Power Conversion Efficiency (PCE) exhibits a pronounced decline with increasing temperature, dropping from a maximum of 24.1% at 275 K to approximately 20.5% at 350 K. This degradation is primarily driven by the reduction in Open-Circuit Voltage (V_{OC}) and Fill Factor (FF), a fundamental behaviour in semiconductors where higher temperatures increase the intrinsic carrier concentration and accelerate non-radiative recombination rates. Interestingly, the Short-Circuit Current Density (J_{SC}) exhibits a linear increase from 40.6 mA/cm^2 to 41.6 mA/cm^2 over the same range. This positive temperature coefficient for current is attributed to the narrowing of the absorber's bandgap at higher temperatures (Varshni effect), which slightly extends the absorption edge towards longer wavelengths. However, the significant losses in voltage and fill factor outweigh the slight gain in current, resulting in an overall negative temperature coefficient for efficiency, which highlights the importance of thermal management for this Sn-based architecture.

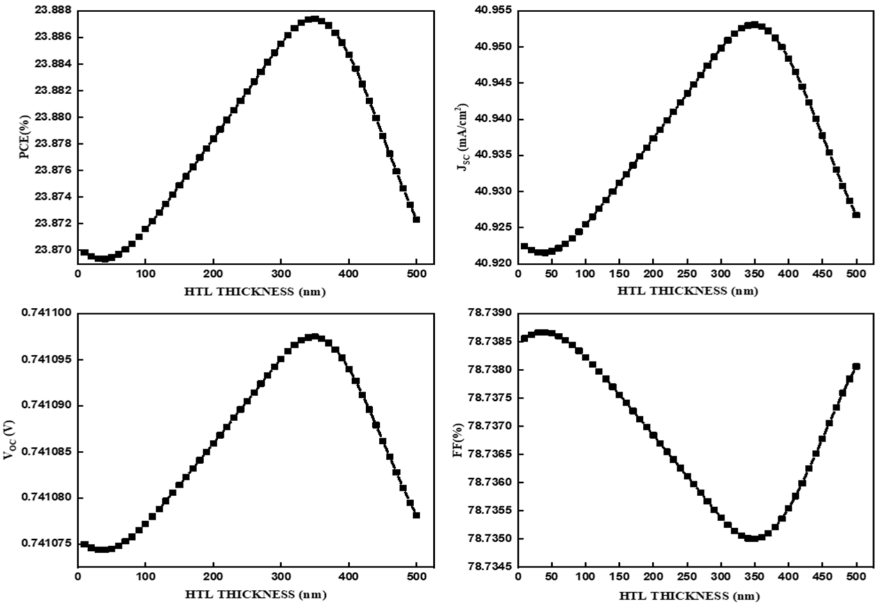

Figure 5. Represents the impact of the Hole Transport Layer thickness on the performance of the PSC.

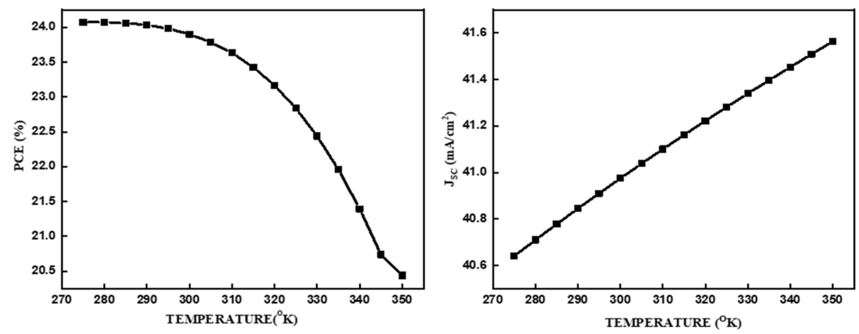

Figure 6. Represents the impact of the Temperature on the performance of the PSC.

Photovoltaic Performance of the Optimised Device Structure:

The photovoltaic performance of the optimised device structure (Glass/FTO/SnS_2/$AZSnBr_3$/$AZSnI_3$/Cu_2O/Au) was analysed under AM 1.5G illumination, as summarised in Figure 7. The Current Density-Voltage (J-V) characteristic (Left) demonstrates excellent diode rectification behaviour with a high Short-Circuit Current Density (J_{SC}) of 41 mA/cm^2 and an Open-Circuit Voltage (V_{OC}) of 0.74 V. The corresponding power density curve (black line) confirms a maximum Power Conversion Efficiency (PCE) peak of 23.9% at a voltage bias of 0.60 V, indicating a high Fill Factor and efficient charge extraction at the maximum power point. Complementing these electrical metrics, the External Quantum Efficiency (EQE) spectrum (Right) reveals a broad panchromatic response, achieving peak conversion efficiencies exceeding 90% in the visible region (400–800 nm). The high EQE values across the spectrum corroborate the exceptional photon harvesting capability of the 15 µm thick absorber layer, while the extended response into the near-infrared region suggests effective utilisation of low-energy photons, consistent with the narrow bandgap nature of Sn-based perovskites.

Table 2. Represents the electrical IV key figures of the optimised structure.

PSC STRUCTURE	PCE (%)	J_{SC} (mA/cm^2)	FF (%)	V_{OC} (V)	EQE (%)
FTO/SnS_2/$AZSnBr_3$/$AZSnI_3$/Cu_2O/Au	**23.91**	**40.99**	**78.73**	**0.74**	**93.68**

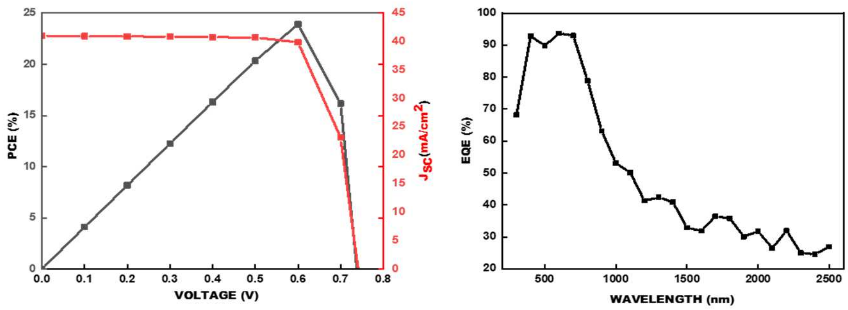

Figure 7. Represents the Optimised PCE and J_{SC} of the PSC structure, b) EQE of the PSC.

CONCLUSION

In this study, we numerically investigated the performance of a lead-free, multi-absorber perovskite solar cell with the configuration Glass/FTO/SnS_2/$AZSnBr_3$/$AZSnI_3$/Cu_2O/Au using the SETFOS-5.3 simulation software. A systematic optimisation of the layer dimensions revealed that the device performance is critically dependent on both optical interference effects and charge transport limitations. An optimised absorber thickness of 15 μm was established, leveraging the saturation of the Short-Circuit Current Density (J_{SC}) to maximise photon harvesting. Furthermore, the thickness of the SnS_2 electron transport layer and the Cu_2O hole transport layer were optimised to 20 nm and 350 nm, respectively, to exploit constructive Fabry-Perot interference patterns that enhance the optical field intensity within the absorber. Under optimised conditions, the device achieved a remarkable Power Conversion Efficiency (PCE) of 23.9%, with a J_{SC} of 40.99 mA/cm^2, a V_{OC} of 0.74 V, and a Fill Factor of 78.73%, supported by an External Quantum Efficiency (EQE) of 93.68% in the visible spectrum. Thermal stability analysis revealed that, while the current density increases slightly with temperature due to bandgap narrowing, the overall efficiency declines to 20.5% at 350 K, primarily driven by the degradation of V_{OC} and fill factor. These findings collectively demonstrate that Azetidinium-based tin perovskites offer a promising, eco-friendly pathway toward high-efficiency photovoltaics, provided that high crystalline quality is maintained to support efficient carrier extraction in thick-film architectures.

ACKNOWLEDGEMENT

This work was supported by the Centre of Excellence in Nano Science and Technology for the Development of Sensors (Co*ENS*Tds), Berhampur University, Odisha, India.

REFERENCES

1. Nelson, Jenny A. *The physics of solar cells*. World Scientific Publishing Company, 2003.
2. Green, Martin A., and Keith Emery. "Solar cell efficiency tables." *Progress in photovoltaics: research and applications* 1, no. 1 (1993): 25-29.
3. Bazilian, Morgan, Ijeoma Onyeji, Michael Liebreich, Ian MacGill, Jennifer Chase, Jigar Shah, Dolf Gielen, Doug Arent, Doug Landfear, and Shi Zhengrong. "Re-considering the economics of photovoltaic power." *Renewable Energy* 53 (2013): 329-338.
4. Green, Martin A. "Photovoltaics: technology overview." *Energy policy* 28, no. 14 (2000): 989-998.
5. Rühle, Sven. "Tabulated values of the Shockley–Queisser limit for single junction solar cells." *Solar energy* 130 (2016): 139-147.
6. Snaith, Henry J. "Perovskites: the emergence of a new era for low-cost, high-efficiency solar cells." *The journal of physical chemistry letters* 4, no. 21 (2013): 3623-3630.

7. Stranks, Samuel D., and Henry J. Snaith. "Metal-halide perovskites for photovoltaic and light-emitting devices." *Nature nanotechnology* 10, no. 5 (2015): 391-402.
8. Kojima, Akihiro, Kenjiro Teshima, Yasuo Shirai, and Tsutomu Miyasaka. "Organometal halide perovskites as visible-light sensitizers for photovoltaic cells." *Journal of the american chemical society* 131, no. 17 (2009): 6050-6051.
9. Green, Martin A., Ewan D. Dunlop, Masahiro Yoshita, Nikos Kopidakis, Karsten Bothe, Gerald Siefer, David Hinken, Michael Rauer, Jochen Hohl-Ebinger, and Xiaojing Hao. "Solar cell efficiency tables (Version 64)." *Progress in photovoltaics: research and applications* 32, no. 7 (2024): 425-441.
10. Park, Nam-Gyu. "Perovskite solar cells: an emerging photovoltaic technology." *Materials today* 18, no. 2 (2015): 65-72.
11. Niu, Guangda, Xudong Guo, and Liduo Wang. "Review of recent progress in chemical stability of perovskite solar cells." *Journal of Materials Chemistry A* 3, no. 17 (2015): 8970-8980.
12. Albrecht, Steve, and Bernd Rech. "Perovskite solar cells: On top of commercial photovoltaics." *Nature Energy* 2, no. 1 (2017): 1-2.
13. Leijtens, Tomas, Kevin A. Bush, Rohit Prasanna, and Michael D. McGehee. "Opportunities and challenges for tandem solar cells using metal halide perovskite semiconductors." *Nature Energy* 3, no. 10 (2018): 828-838.
14. Dikhit, Arati, and Sukanta Kumar Tripathy. "Enhancing the solar cell efficiency with Azetidinium based Perovskites: An investigation for device optimization using DFT and SETFOS." *Solar Energy* 284 (2024): 113089.
15. Pering, Samuel R., Wentao Deng, Joel R. Troughton, P. S. Kubiak, D. Ghosh, R. G. Niemann, F. Brivio et al. "Azetidinium lead iodide for perovskite solar cells." *Journal of Materials Chemistry A* 5, no. 39 (2017): 20658-20665.